STATISTICALLY AND BIOMECHANICALLY BASED CRITERION FOR IMPACT-INDUCED SKULL FRACTURE

Michael Vander Vorst, James Stuhmiller, and Kevin Ho
Jaycor, Inc.

Narayan Yoganandan and Frank Pintar
Medical College of Wisconsin

ABSTRACT

This work developed a skull fracture criterion for impact-induced head injury, using post mortem human subject tests, anatomical test device measurements, statistical analyses, and finite element modeling. It is shown that skull fracture correlates with the tensile strain in the outer table of the cranial bone, and an index termed the Skull Fracture Correlate (SFC) predicts injury. SFC offers several advantages as a protection criterion. It accounts for compliance of the impact site; it is extensible to varying head mass; and it is easily implemented using current software. For a 15% or less probability of skull fracture the criterion is SFC < 120 g, with a 95% confidence band of 88 < SFC < 135 g.

The growing understanding of head injuries indicates that a comprehensive assessment of impact-induced injuries involves many modes, each requiring a specific criterion. Although Europe, Japan, Australia, and the United States have adopted the Head Injury Criterion (HIC) as a standard for impact protection in motor vehicle collisions, research is far from complete on defining the best index to predict all modes of injury. Experimental and mathematical studies are ongoing, such as those presented at IRCOBI [e.g., Kleiven and von Holst, 2001], Stapp [e.g., Newman, 2000], and AAAM. Each of the many modes of head injury is governed by a different injury mechanism. For example, skull fracture is related to skull strain [Wood, 1971], subdural hematoma is due to the rupture of bridging veins [Meaney, 1991], and diffuse axonal injury results from axonal strain [Thibault, et al., 1982]. A multimode approach to

predict head injury is needed. This research addresses one mode of head injury - impact-induced linear skull fracture. Impact skull fracture depends on both the geometry and compliance of the impact material (the target) and the weight of the head. Together, these factors determine the stress and strain distributions generated in the skull. Fractures occur at lower impact speeds against harder targets than softer ones [Hodgson and Thomas, 1973]. For fixed impact speed and target, a heavier head will experience greater contact forces, and therefore, larger stresses and strains in the skull than a lighter one. Fracture occurs when the ultimate strain is exceeded.

Previous work of Hodgson and Thomas (1971 and 1973) provides fracture outcomes for varying impact speeds, target compliances, and surface curvatures. In their tests, embalmed whole body Post Mortem Human Subjects (PMHS) were placed on a hinged pallet pivoted at the feet of the specimen, with the head extending over the edge. The forehead impacted at the point of highest curvature. Known head weights varied between 3.2 and 5.4 kg with an average of 4.7 kg, which is close to the 4.5 kg weight of the 50^{th} percentile male Hybrid III headform specified by FMVSS 208 for use in car crash tests. In many cases the head weight was not recorded. Impacts against flat targets, cylinders with large radius of curvature, and rubber targets produced primarily linear skull fracture while impact against rigid hemispheres and rigid cylindrical targets with small radius of curvature produced comminuted fracture. Impact speeds varied within ±20% of the theoretical free drop value with an average near zero and a standard deviation of 8%.

More PMHS data are needed to extend the validity of injury criteria to a wider population group and a wider range of target compliance. At present, skull fracture data outside the scope of Hodgson and Thomas' tests are limited. Hodgson and Thomas' tests provide fracture data for, on average, 50^{th} percentile male subjects. To extend injury criteria to other adult populations, new tests are needed with lighter weight specimens. Hodgson and Thomas' use of a rotating pallet resulted in a large variation in impact speed and limited the drop height to 1.2 m. Free drops of isolated head specimens would provide accurate specification of impact conditions and allow for higher impact speeds. The softest target used by Hodgson and Thomas was durometer 60 neoprene. The fracture criterion should be extended to more compliant targets. This work presents results of new skull fracture tests using free drops of isolated, light-weight, unembalmed specimens impacted against a wide range of targets.

Since regulatory crash tests require Anthropomorphic Test Devices (ATDs) as human surrogates, the development of injury criteria for crashworthiness tests must be based on ATD measurements, while pathological outcomes are obtained from laboratory tests with biologic specimens. The relationship between PMHS skull fracture and risk factors computed from measured ATD response can be established using statistical correlations. The search for the best risk factor, however, must be guided by a biomechanical understanding of the underlying injury mechanism. In the case of the human skull, tensile strain in the compact tables is an indicator of fracture [Wood, 1971], but skull strain data at the location of fracture is difficult to measure in an impact test and in any case is not available for historical test data. However, strain can be calculated with a finite element model using the PMHS test conditions as input.

Modeling is a useful tool to advance the fundamental biomechanical understanding of injury mechanisms and as an aid in expanding injury criteria to other population groups. Models can be used to predict variables that cannot be measured from PMHS specimens. Finite element models of varying complexity exist for the investigation of head injury: from highly refined whole-head models containing hundreds of thousands of elements [Zhang, et al., 2001], to anthropomorphically correct models containing tens of thousands of elements concentrating on resolving the skull [Bandak and Vander Vorst, 1995], to simple spherical models containing thousands of elements [Khalil and Hubbard, 1977]. Since this research is concerned with local strain distribution about a single point of impact, a simple spherical model similar to that of Khalil and Hubbard, with a sufficient number of elements to resolve the geometry about the impact area and with material properties sufficient to capture the mechanical response, would provide an understanding of the underlying biomechanics.

The objective of this research is therefore to develop a statistically- and biomechanically-based criterion to frontal, impact-induced, linear skull fracture for crashworthiness tests. Risk factors calculated from ATD response data are correlated to skull fracture outcomes, and the biomechanical basis is established using finite element model simulations validated against PMHS data. To accomplish this objective, new PMHS tests are conducted to provide linear skull fracture outcomes over a range of conditions beyond that available from the literature; drop tests with a Hybrid III headform are performed to provide ATD-based kinematic and dynamic risk factors; and finite element simulations are performed to compute the tensile strain in the skull corresponding to each of the PMHS tests.

The progression of this research is to (1) obtain skull fracture data from the open literature and from new PMHS tests; (2) compute candidate risk factors from measurements of drop tests with a Hybrid III headform under the same conditions as the PMHS tests; (3) compute tensile skull strain corresponding to each PMHS test with a finite element head model; (4) using the skull fracture data from the open literature, determine the risk factor that is the best correlate to skull fracture; (5) validate this final correlate with new PMHS test data; and (6) establish the biomechanical validity of the final risk factor by comparing it to computed tensile strain.

METHODS

Frontal impact test cases exhibiting primarily linear skull fracture were extracted from the Hodgson and Thomas (1971 and 1973) data set. Tests against slender rods and hemispheres were excluded since they resulted in depressed comminuted fractures instead of the linear fractures caused by the flat and 5-cm diameter cylindrical targets. Anomalous cases, as reported by Hodgson and Thomas, were also excluded. This extracted data set was used to determine the skull fracture correlates for the 50^{th} percentile male. Logistic regression analysis was performed using Stata (1999) and the Hosmer-Lemeshow (1989) goodness-of-fit statistic, G, and 95^{th} percentile confidence bands were determined. G varies between zero and one with the value one for a fit were all data falls on the regression line.

To validate the injury correlates and expand the range of head weights and impact conditions beyond that of Hodgson and Thomas, drop tests were conducted at the Medical College of Wisconsin using isolated PMHS head specimens. These tests are hereafter referred to as the MCW tests. Six unembalmed specimens, free from HIV, and Hepatitis B and C were obtained. The craniums, along with the intracranial contents, were used as test specimens (Table 1). The Institutional Review Board of the Medical College of Wisconsin approved the protocol. Pretest radiographs and Computed Tomography (CT) images of the specimens were obtained. Forehead impact tests were conducted by dropping the specimens against either flat, 5-cm thick 40-, or 90 durometer impact targets at velocities ranging from 2 to 10 m/s. Three specimens impacted the durometer 40 target and three impacted the durometer 90 target. Each specimen was impacted at increasing heights with a single impact at each height, and radiographs were obtained between drops. Testing of a specimen was terminated when fracture was detected using x-rays, the impact force decreased with increasing drop height, or the load cell reached its design limit of 9 kN. Impact force histories were recorded using a six-axis load cell. Signals were recorded using a digital data acquisition system (DTS Technologies, Seal Beach, CA) according to the 1998 Society of Automotive Engineers Specifications at a sampling frequency of 12.5 kHz and filtered according to SAE Channel Class 1000 specifications [SAE, 1995]. The specimens underwent CT scanning after the final impact. The MCW tests were used to extend the validity of the correlations to softer targets and lighter heads. They included softer targets, durometer 90 and 40, compared to the rigid, durometer 90 and 60 targets used by Hodgson and Thomas; and the tests used lighter heads than the 4.5 kg 50th percentile male (Table 1).

Table 1 – Subject Data for MCW Skull Fracture Tests

ID	Sex	Age	Head Weight (kg)	Head Circ. (mm)	Head Height (mm)	Head Width (mm)	Head Length (mm)	Stature (m)
1	F	67	2.5	530	178	152	191	1.68
2	F	83	2.1	508	159	140	184	1.52
3	F	65	2.5	508	178	152	162	1.65
4	M	56	2.8	565	152	146	203	1.78
5	M	78	3.3	546	178	146	178	1.78
6	M	75	3.3	533	165	152	197	1.70

To obtain kinematic and dynamic risk factors for injury correlation, drop tests using a 50th percentile male Hybrid III headform were conducted corresponding to each PMHS test condition in the selected Hodgson and Thomas tests and in the MCW tests (Figure 1). Three repeated drops were made for each impact condition. Maximum contact area between the headform and the target was obtained using Pressurex pressure sensitive film with a range of 190 to 540 kPa. Accelerations at the center-of-gravity of the headform were measured and filtered to meet SAE J211 Channel Class 1000 specifications for impact tests. Impact force was measured by a Kistler model 925M113 force gauge affixed to a 30-cm deep concrete slab below the target mount. Data were recorded at a rate of 50 kHz using the National Instrument LabVIEW system and processed to give candidate kinematic and dynamic risk factors for skull fracture. Dynamic risk factors included impact area and peak force. Kinematic risk factors included HIC, the peak acceleration, A_{max}, the average acceleration over the entire contact time, A_{av}, and the average acceleration, A_{HIC}, over the HIC time interval.

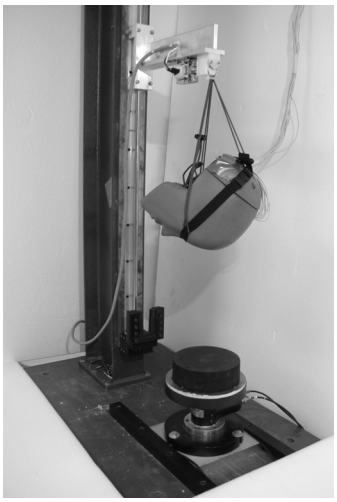

Fig. 1 – Hybrid III headform on drop assembly with target

HIC was calculated as

$$HIC = \left[\frac{1}{(t_2 - t_1)} \int_{t_1}^{t_2} a\,dt \right]^{2.5} (t_2 - t_1) \qquad (1)$$

where the resultant acceleration, a, is in units of g, and "t_1 and t_2 (in seconds) are any two points in time during the crash of the vehicle" [USCFR FMVSS 208, 2002]. The time interval, ΔT_{HIC}, that maximizes the integral in Equation 1 is

$$\Delta T_{HIC} = (t_2 - t_1), \qquad (2)$$

and the change in velocity, ΔV_{HIC}, over that interval is

$$\Delta V_{HIC} = \int_{t_1}^{t_2} a\,dt\ . \qquad (3)$$

HIC and A_{HIC} are then expressed as

$$HIC = (\Delta V_{HIC})^{2.5} / (\Delta T_{HIC})^{1.5}\ , \text{ and} \qquad (4)$$

$$A_{HIC} = \Delta V_{HIC} / \Delta T_{HIC}\ . \qquad (5)$$

Repeated tests were checked for consistency and computed risk factors were averaged over repeated tests for statistical analysis. Peak accelerations were verified against the ratio of force to headform weight.

A nonfracturing, spherical, finite element skull model was constructed to simulate skull impact (Figure 2). Maximum principal tensile strain in the compact skull tables was calculated for the same impact conditions as the PMHS tests. The model was composed of 15,200 brick elements. Skull material properties were taken from Khalil and Hubbard (1977), and brain material properties were taken from Bandak and Eppinger (1994), (Table 2). Brain density was used to adjust head weight. Scalp was assumed to be linear viscoelastic with material properties obtained by calibrating the calculated acceleration with the measured response from 38 cm PMHS drop tests onto a flat rigid plate. Material properties for the neoprene targets were assumed to be linear viscoelastic with bulk modulus of 1.4 GPa. Long-term neoprene shear moduli were determined by conducting force displacement tests. Short term shear moduli and decay rates were calibrated by adjusting these parameters until the computed acceleration response matched the acceleration response from drop tests of a 4.5 kg, 18 cm-diameter rigid sphere against the neoprene targets. All finite element model simulations were performed using Version 9.60 of LS-Dyna3d software [LSTC, 2002].

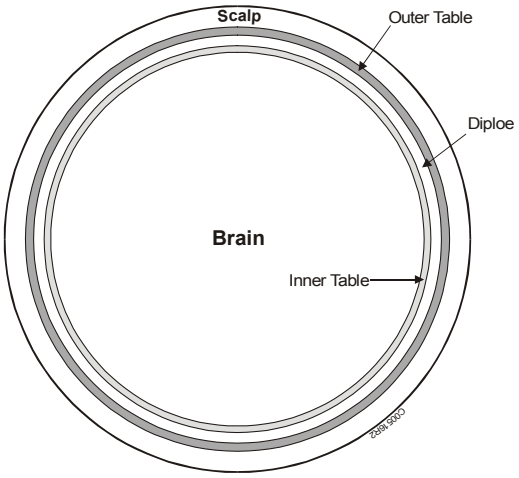

Fig. 2 – Three-dimensional spherical head model

Table 2 – Material Properties of Finite Element Model

Property	**Value**
Brain	
Diameter	14 cm
Specific gravity	1.0
Bulk modulus	2.04 GPa
Short term shear	68 kPa
Long term shear	34 kPa
Decay time	0.01 sec
Skull	
Thickness	
Outer table	1.5 mm
Diploe	3.0 mm
Inner table	1.5 mm
Specific gravity	
Table	2.9
Diploe	1.7
Young's modulus	

Property	Value
Table	16 GPa
Diploe	0.73 GPa
Poisson's ratio	
Table	0.35
Diploe	0.05
Scalp	
Thickness	6.1 mm
Specific gravity	1.2
Bulk modulus	6.8 MPa
Short term shear	*
Long term shear	*
Decay time	*
Summary	
Diameter (in.)	16 cm
Weight	4.5 kg

* Determined by calibration (see Methods and Table 5 of Results).

RESULTS

Three of the six MCW PMHS specimens were tested to fracture (Table 3). Following the test protocol, testing of Specimen 2 and 5 was terminated because the peak force decreased; however, final pathology revealed no fractures in Specimen 5. Testing of Specimens 3 and 6 was terminated because the force gauge reached its design limit. Skull fractures were primarily linear in nature (Figure 3). All time history shapes were similar, with pulse durations decreasing with increasing impact velocities for specific padding.

Table 3 – Outcomes from MCW PMHS tests

Specimen ID	Target	Height (m)	Time Period (ms)	Fracture
1	5 cm thick flat durometer 90 (D90) neoprene	0.30	4.2	No
		0.61	3.9	No
		0.91	3.7	No
		1.22	4.1	Yes
2	5 cm flat D90	0.30	4.1	No
		0.61	3.8	No
		0.91	3.8	No
		1.22	4.5	Yes
3	5 cm flat D90	0.30	4.1	No
		0.61	3.7	No
		0.91	3.5	No
		1.22	3.7	No

Specimen ID	Target	Height (m)	Time Period (ms)	Fracture
4	5 cm flat D40	0.61	10.2	No
		0.91	10.4	No
		1.52	9.5	No
		1.83	9.0	No
		2.13	8.8	No
		2.44	8.0	No
		2.74	8.4	No
		3.05	8.4	Yes
5	5 cm flat D40	1.22	10.4	No
		1.83	8.4	No
		2.13	9.4	No
6	5 cm flat D40	1.22	10.6	No
		1.52	10.1	No
		1.83	9.6	No
		2.13	9.6	No
		2.44	9.4	No
		2.74	9.3	No
		3.05	9.1	No

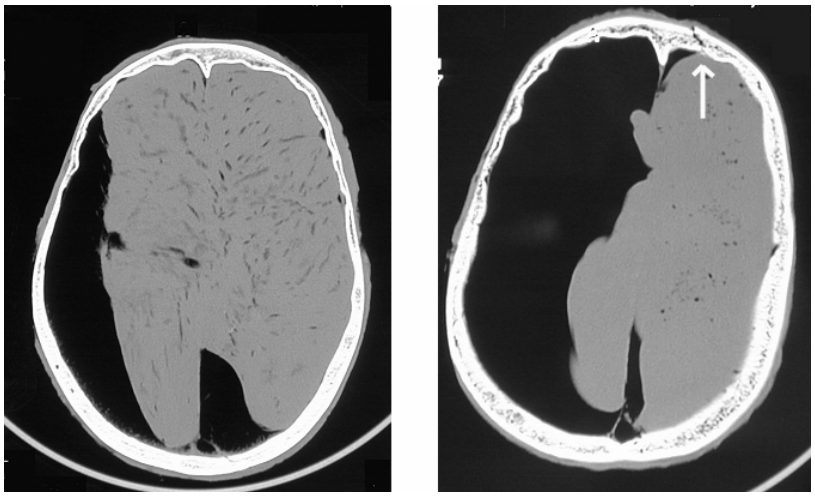

(a) Pretest scan (b) Post test scan showing fracture

Fig. 3 – CT Images of Test Specimen

A database of PMHS skull fracture outcomes with corresponding risk factors from Hybrid III headform drop tests was constructed for statistical analysis. Data for the 30 MCW PMHS tests and 76 tests selected from Hodgson and Thomas (1971 and 1973) were entered into the database (Tables 3 and 4). The Hodgson and Thomas data were used to develop the regressions and the MCW data were used to validate them.

Table 4. Test Conditions from Hodgson and Thomas

Impact Target/ Drop Height	13 cm	15 cm	25 cm	30 cm	38 cm	51 cm	61 cm	64 cm	76 cm	91 cm	112 cm	122 cm	127 cm
Flat rigid	x	x	x					x	x				
Flat durometer 90				x	x		x			x	x		
Flat durometer 60			x	x	x	x	x		x	x		x	x
5 cm diameter rigid cylinder, transverse			x		x	x		x	x				
5 cm diameter rigid cylinder, sagittal	x		x		x	x			x				
5 cm diameter durometer 90 cylinder, sagittal				x	x		x			x		x	
5 cm diameter durometer 60 cylinder, sagittal			x			x			x			x	

"x" indicates Hybrid III headform drop test performed

Figure 4 shows transient CG acceleration waveforms for Hybrid III headform and corresponding PMHS drops onto targets with varied compliance. The PMHS and Hybrid III acceleration responses are in good agreement for these non-fracturing cases. All curves are unimodal. Impact durations vary between 3 and 8 ms with the shortest time duration for the rigid target and longest for the most compliant target.

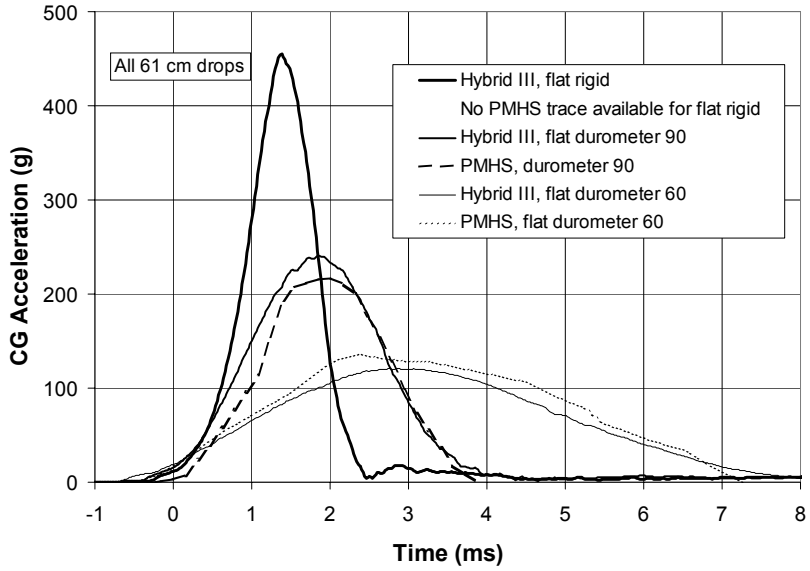

Fig. 4 – Hybrid III and PMHS CG Acceleration by Impact Target

The calibrated viscoelastic material properties of the neoprene targets and those of human scalp used in the finite element model are given in Table 5.

Table 5. Calibrated Viscoelastic Material Properties

Material	Long Term Shear Modulus (MPa)	Short Term Shear Modulus (MPa)	Decay Rate (ms)
Human scalp	2.7	0.68	0.17
Durometer 90 neoprene	36	12	1.2
Durometer 60 neoprene	5.4	2.7	1.1
Durometer 40 neoprene	5.4	2.3	1.1

Force was not considered in the regression analysis since force/mass was nearly identical to acceleration. Peak force is a near perfect correlate to peak acceleration. The acceleration predicted by the model was also similar to the measured Hybrid III headform acceleration. In addition, the acceleration and strain waveforms from the model had similar shape, with peak strain occurring at nearly the same time as peak acceleration.

Peak skull tensile strain, computed by the finite element model, was a statistically significant correlate with skull fracture,

$$\ln[P/(1-P)] = 5.89*\ln(\text{strain}) + 12.582, \quad (6)$$

where P is the probability of fracture (Figure 5). The strain at 50% probability of fracture is 0.12% and the goodness-of-fit statistic, G, is 0.17.

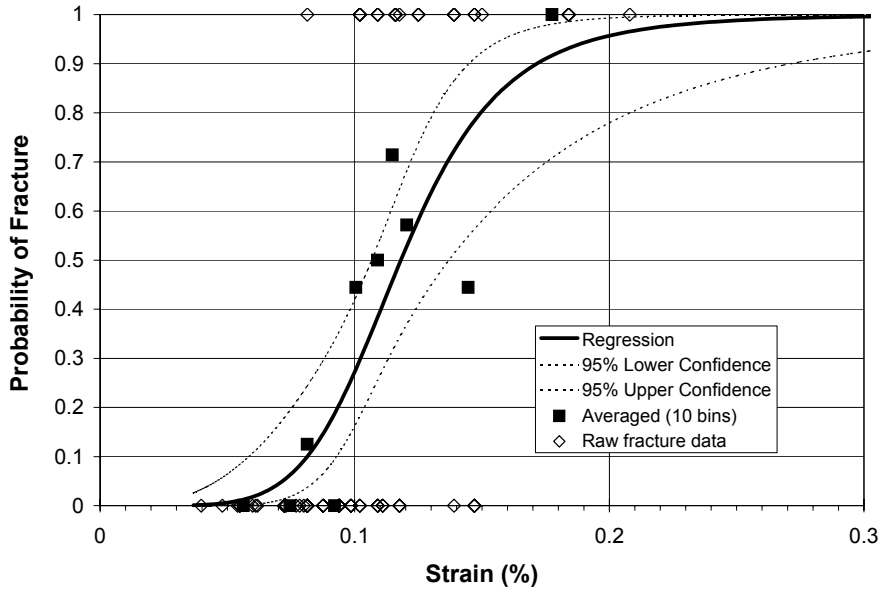

Fig. 5 – Logistic Regression of Strain to Skull Fracture

A_{HIC} was the best correlate to skull fracture (Table 6, Figure 6). The risk factors A_{HIC}, A_{max}, A_{av} and HIC were each statistically significant correlates; however, only A_{HIC} remained after backwards step-wise elimination. A_{HIC} has the highest goodness-of-fit. Area was not statistically significant; however, when combined with HIC, it was retained by stepwise elimination yielding the risk factor $HIC/Area^{0.910}$ (Table 6). Conversely, area was eliminated when used with A_{HIC}. Regression to the bivariate combination of ΔV_{HIC} and ΔT_{HIC} gave the risk factor $\Delta V_{HIC}/(\Delta T_{HIC})^{1.02}$, which was remarkably similar to A_{HIC} (Table 6, Eq. 5). The confidence band of the A_{HIC} regression is well behaved widening slightly at high probability of fracture (Figure 6). Conversely, the HIC correlation exhibits a steep rise at low probability with a significantly wider confidence band at high probability of fracture (Figure 7).

Table 6. Logistic Rregressions to Skull Fracture
($p < 0.000005$ for all regressions)

Correlations with ln[P/(1-P)]	Risk Factor	G
$5.293*\ln(A_{HIC}) - 27.021$	A_{HIC}	0.24
$5.212*\ln(\Delta V_{HIC}) - 5.313*\ln(\Delta T_{HIC}) - 27.231$	$\Delta V_{HIC} / \Delta T_{HIC}^{1.02}$	0.24
$2.035*\ln(HIC) - 13.586$	HIC	0.21
$2.843*\ln(A_{av}) - 11.898$	A_{av}	0.19
$5.337*\ln(A_{max}) - 28.430$	A_{max}	0.06
$3.007*\ln(HIC) - 2.735*\ln(Area) - 12.665$	$HIC/Area^{0.910}$	0.03

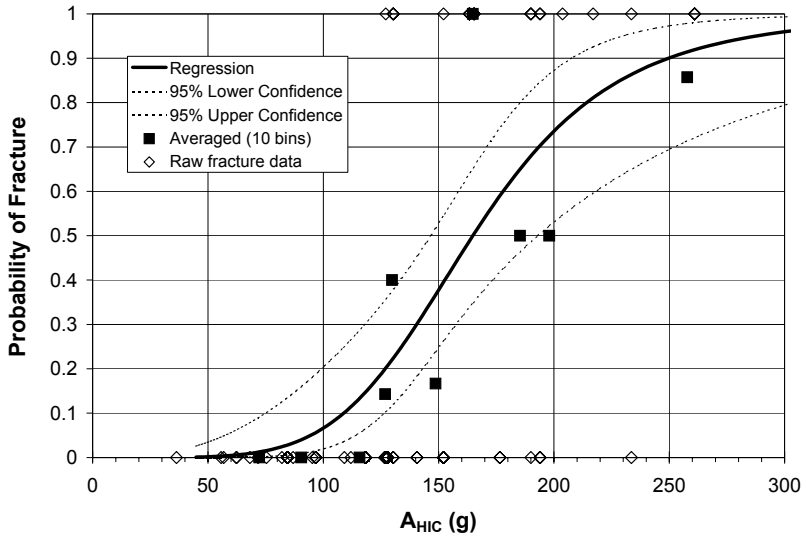

Fig. 6 – Logistic Regression of A_{HIC} to Skull Fracture

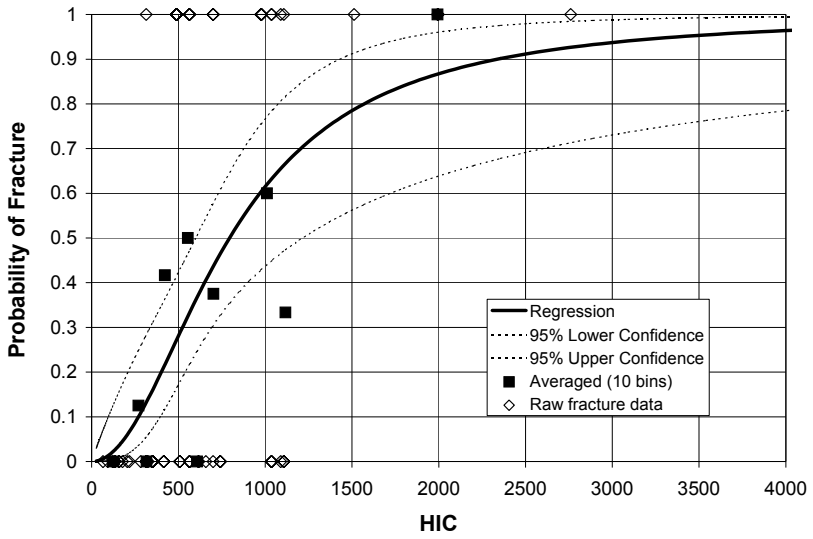

Fig. 7 – Logistic Regression of HIC to Skull Fracture

The biomechanical basis of A_{HIC} is firmly established by its excellent correlation with computed strain showing the highest R^2 among all the risk factors (Table 7). Cross-plotting A_{HIC}, A_{max}, and $HIC/Area^{0.91}$ against strain by target compliance revealed that these correlations were invariant with compliance as illustrated for A_{HIC} (Figure 8) and $HIC/Area^{0.91}$ (Figure 9). Conversely the correlation of HIC to strain varies with target compliance (Figure 10); showing that HIC is not a biomechanically consistent risk factor for skull fracture. HIC values at 50% probability of fracture were 500, 650, and 1240 for flat rigid, durometer 90, and durometer 60 targets respectively. This dependence of target compliance on HIC occurs even though the R^2 of the correlation of HIC with strain is 0.88 (Table 7). This demonstrates the importance of evaluating risk factors against a biomechanical basis and not relying solely on statistical analysis.

Table 7 – Correlations of Risk Factors with Strain

Risk Factor	**Correlation with strain (power law fit)**	**R^2 (all data)**
A_{HIC}	$0.0026*A_{HIC}^{0.765}$	0.92
A_{max}	$0.0020*A_{max}^{0.767}$	0.91
HIC	$0.085*HIC^{0.3957}$	0.88
$HIC/Area^{0.910}$	$0.0234*(HIC/Area^{0.910})^{0.381}$	0.78
A_{av}	$0.0127*A_{av}^{0.530}$	0.76

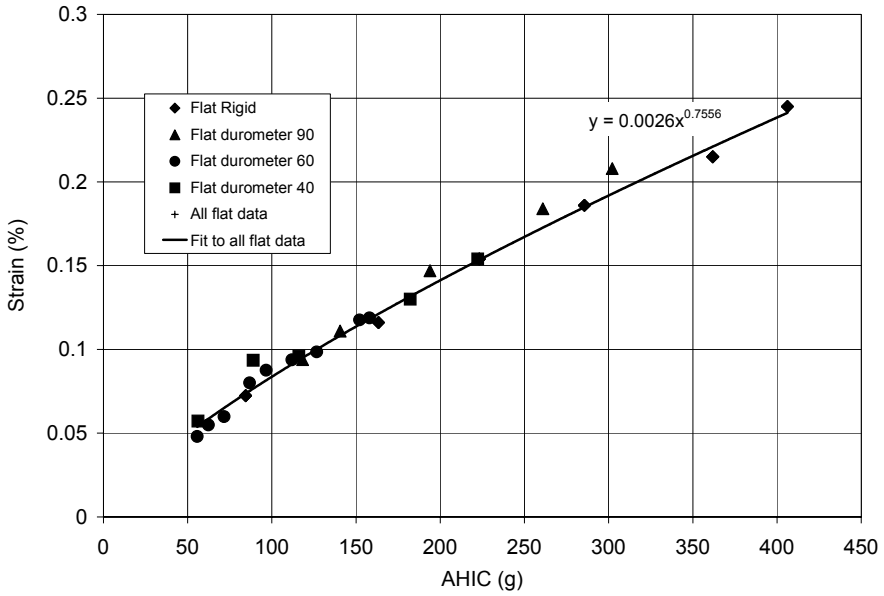

Fig. 8 – A_{HIC} vs. Strain by Target Compliance

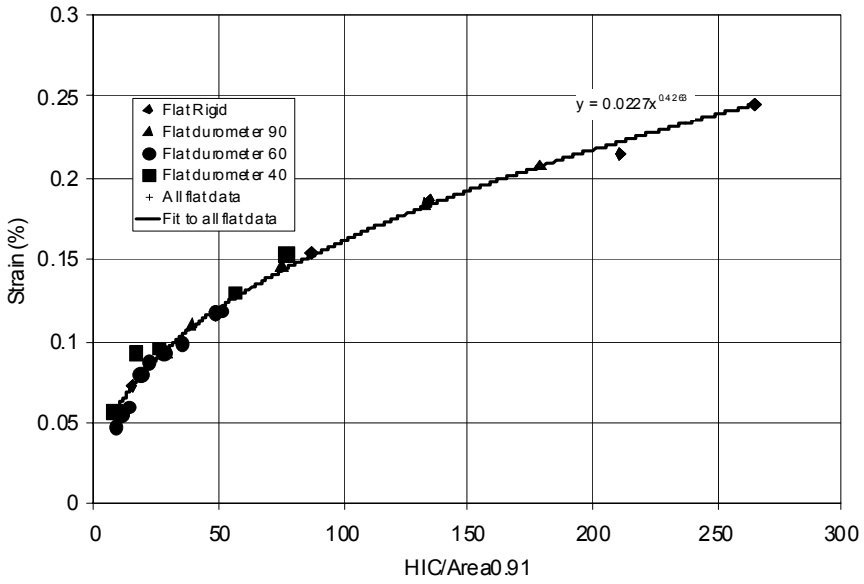

Fig. 9 – HIC/Area$^{0.91}$ vs. Target Compliance

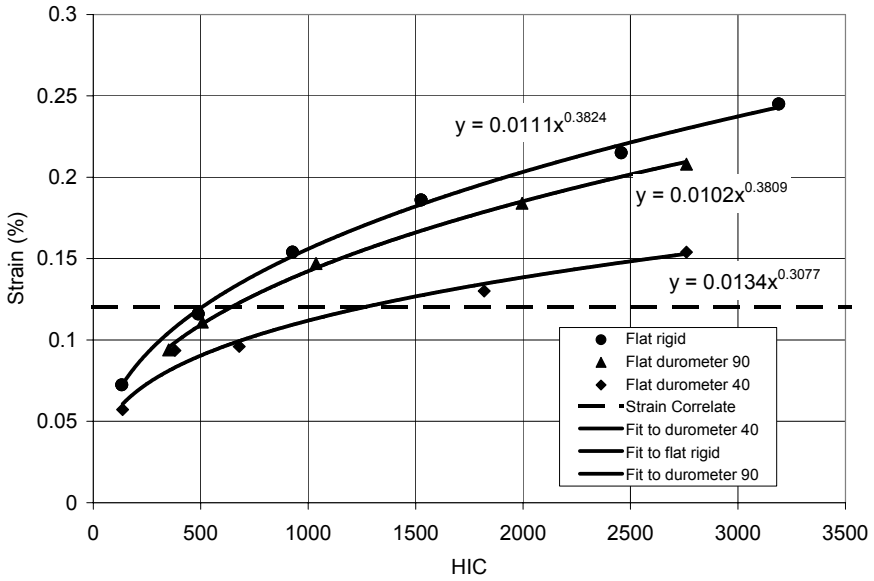

Fig.10 – HIC vs. Strain by Target Compliance

When A_{HIC} is scaled by the specimen mass relative to the Hybrid III headform mass, strain versus A_{HIC} for the MCW PMHS tests showed good agreement with the A_{HIC} regression (Figure 11). Hence, the MCW tests with mass scaling validated the regression of A_{HIC} to skull fracture over a range of head weights and material compliances outside that used to determine the regression. The average head weight of 2.8 kg in MCW tests was only 60% of that in the Hodgson and Thomas tests. Also, the lowest compliance targets in the MCW tests were softer, durometer 40 neoprene compared to durometer 60 used in the Hodgson and Thomas tests.

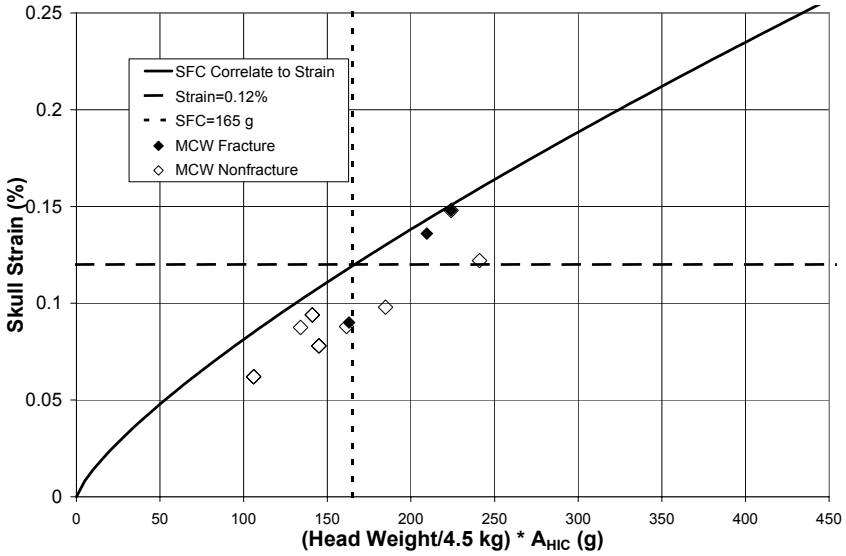

Fig. 11 – A_{HIC} vs. Strain after Scaling by Head Weight

The 50% probability of frontal impact skull fracture occurs at

$$A_{HIC50} = 165 \text{ g},$$

when measured by the Hybrid III headform. Removing the logarithms in the logistic equation for A_{HIC} (Table 6) gives

$$P/(1-P) = [A_{HIC} / A_{HIC50}]^{5.29}. \quad (7)$$

A_{HIC} at 15% probability of skull fracture is

$$A_{HIC15} = 120 \text{ g},$$

with 95% confidence band (Figure 7) of

$$88 < A_{HIC15} < 135 \text{ g}.$$

DISCUSSION

Of the risk factors considered, A_{HIC} is the best biomechanically based correlate to frontal, impact-induced, linear skull fracture as confirmed by backward stepwise elimination. A_{HIC} is also the risk factor with the best correlation to computed tensile skull strain and is invariant with contact area, capturing the contribution of contact area to fracture, and hence obviating the need for the measurement of contact area in crash tests. Since A_{HIC} is $\Delta V_{HIC}/\Delta T_{HIC}$, the averaged acceleration over the HIC time interval, it is easily calculated from measurements and software algorithms currently in use. The quantity A_{HIC} will hereafter be referred to as the Skull Fracture Correlate, SFC, where

$$SFC = A_{HIC} = \Delta V_{HIC}/\Delta T_{HIC}. \quad (8)$$

Hence, SFC, the average acceleration over the HIC interval, is the best correlative risk factor to frontal impact-induced linear skull fracture and it is also a near perfect cross-correlate with skull strain, a biomechanical measure of skull fracture.

HIC, by itself, is a poor predictor of skull fracture due to its inadequate capturing of impact area effects. This was shown by the retention of area with HIC during backward stepwise elimination, which resulted in the risk factor $HIC/Area^{0.91}$. Without the contribution of impact area, the HIC correlation with strain varies strongly with target compliance, giving multiple threshold values for different targets. However, the risk factor, of $HIC/Area^{0.91}$ requires the impact area, a quantity not easily measured in crash tests.

The Wayne State Tolerance Curve (WSTC) [Patrick et al., 1963], upon which HIC is based, was developed to provide a single criterion for both skull fracture and concussion with acceleration time durations varying from 3 to 50 ms. Tests upon which the WSTC are based were against only a flat rigid target. In comparison, SFC is valid for both rigid and compliant targets of varying shapes and is limited to skull fracture.

Comparison of SFC against the MCW data shows that SFC can be extended to other population groups using mass scaling. SFC as expressed in Equation (7) applies to the 50^{th} percentile male. However, the average head mass of the MCW tests was about 60% of that of the 50^{th} percentile male Hybrid III headform. As shown by its correlation with strain, SFC can be scaled to other population groups as

$$SFC(M) = (M_0/M)*SFC, \quad (9)$$

where M is the actual skull mass and M_0 is the mass of the 50^{th} percentile male Hybrid III headform (Figure 11). This result predicts that lighter heads fracture at higher SFC, because the impact force, and hence, the skull stress and strain is lower for the lighter heads. The effect of variation in skull thickness and of the difference between male and female specimens was not investigated since skull thickness measurements were not generally available and most of the specimens in the Hodgson and Thomas tests were male. The mass scaled values of SFC(M) used in the validation appear somewhat below the SFC-strain correlation, although the overall comparison is excellent (Figure 11). The discrepancies may be due to differences between the Hodgson and Thomas tests and the MCW tests. The Hodgson and Thomas tests used a hinged pallet holding the whole cadaver, while the MCW tests used isolated specimens. In addition, the Hodgson and Thomas tests used embalmed subjects while the MCW specimens were unembalmed. Even though the two test protocols were significantly different, it is encouraging to see their agreement when head mass is accounted for. We consider that more data are needed to refine the extension of SFC to other population groups.

The present finite element model, whose purpose is to investigate the biomechanical consistency of measurable risk factors to skull fracture, is a simplified spherical model that essentially calculates the average strain distribution in the skull. Higher stress/strain concentrations due to complexities of the bone structure and variation in material properties will not be captured. Based on Wood's (1971) study from mechanical testing of 118 specimens, the breaking strain of the compact layers of human skull bone was strain rate dependent with ultimate strain,

$$\varepsilon_{ult} = (0.63 - 0.04 \log \varepsilon') \%. \quad (10)$$

For the present data set, the strain loading rate, ε', varies between approximately 0.1 to 2 sec^{-1} (Figure 4). In this range the breaking strain, ε_{ult}, is nearly constant, varying between 0.62% and 0.67%, which is greater than the strain of 0.12% at 50% probability of fracture calculated by the spherical finite element model. This discrepancy is not surprising and is probably due to the inherently stronger nature of the spherical head model since it does not account for stress concentrations due to local curvature and thickness variations. However, it is significant that the calculated strain shows an excellent correlation with SFC (Figure 8), providing a strong biomechanical basis for the correlation.

In the present model, the material properties of the skull bone were assumed to be linearly elastic. Elasticity of the compact skull tables is strain rate dependent [Wood, 1971],

$$E = (2.32 + 0.28 \log \varepsilon') \text{ Mpsi}, \quad (11)$$

over a strain rate from 0.05 to 200 sec^{-1}. However for the strain loading rates of 0.1 to 2 sec^{-1} (Figure 4) in this study, the elasticity varies by less than 10% from the mean, an amount presumably much less than the physical variability of individual specimens. Hence, the viscoelastic effect was accounted for in the model by using a linear elastic modulus approximating the mean viscoelastic modulus over the strain rates of interest.

Viscoelastic material properties of the neoprene impact targets and of human scalp were calibrated only over the range of test conditions in this research. These may not be the most general formulations.

Because of the biological nature of the experimental model, fracture was not sustained at the same level of impact velocity for a given target (Table 3). For example, with the durometer 90 target, specimens 1 and 2 sustained fractures at a drop height of 1.22 m (velocity 4.9 m/s) while fracture was not sustained in specimen 3. Fracture pathology determined specimen failure. Presence of microfractures has been identified in bony structures including the human spinal column [Yoganandan et al., 1988, and Yoganandan et al., 1989]. Although such fractures can go undetected in radiographic images, the determination was made to define skull fracture as that detectable by radiographic methods. Microfractures would not receive treatment in a clinical setting, whereas fracture detected on x-ray is clinically relevant and better defined for biomechanical analysis. It is not the purpose of this study to detect such microlevel trauma in isolated specimens. At the macrolevel, since all curves exhibited similar shapes (Table 3), only results of pathological observations were used to meet the objectives of the study.

Even though the pressure sensitive film measures the cumulative area of impact, for the tests in this work, the film provides a good measure of the peak contact area with respect to time, since inspection of high-speed movies of the Hybrid III headform impacts show little rotation during impact.

The major limitation of this work is that the results are for frontal, impact-induced, linear, skull fracture in crashworthiness testing. Other impact locations such as the parietal, temporal and occipital bones were not considered nor were other fracture types, such as local comminuted or depressed fractures.

CONCLUSION

The results of this work lead to SFC, the average acceleration over the HIC time interval, as the best correlate to frontal, impact-induced, linear skull fracture for crashworthiness assessment. Its biomechanical basis is established by its excellent correlation with skull strain. SFC offers several advantages as a useable protection criterion:

1. It accounts for hard and soft impact targets.

2. It can be extended to varied head weights.

3. It is easily implemented using current software algorithms.

The criterion that the probability of skull fracture is less than 15% is

$$SFC < 120 \text{ g},$$

with a 95% confidence band of

$$88 < SFC_{15} < 135 \text{ g}.$$

ACKNOWLEDGMENTS

This study was supported by the National Highway Traffic Safety Administration (NHTSA), U.S. Department of Transportation through a Joint Cooperative Research Agreement with the U.S. Army Medical Research and Materiel Command under contract DAMD17-93-C-3005.

The authors thank Faris Bandak, Senior Science Advisor, Directorate of Safety and Security for Volpe National Transportation Systems Center, for his encouragement and support during the early phase of this research. We also thank our NHTSA program managers: Rolf Eppinger, Erik Takhounts, Peter Martin and Matt Maltese for their kind support and Philemon Chan of Jaycor for his guidance and advice.

REFERENCES

Bandak, F.A. and Eppinger, R.H. "A Three-Dimensional Finite Element Analysis of the Human Brain under Combined Rotational and Translational Accelerations," SAE paper 942215, 38th Stapp Car Crash Proceedings, P-279; 1994.

Bandak, F.A. and Vander Vorst, M.J. "An Imaging-Based Computational and Experimental Study of Skull Fracture: Finite Element Model Development." J. Neurotrauma, 12(4): 679-688; 1995.

Eppinger, R.A. and Takhounts, E.G. "On the Development of Survival Criteria for Rate Sensitive Materials." 44th Stapp Car Crash Conference, SAE 2000-01-SC04, 2000.

Hodgson, V.R. and Thomas, L.M. "Breaking Strength of the Skull vs. Impact Surface Curvature," DOT HS-800 583, Contract No. FH-11-7609, Final Report; 1971.

Hodgson, Voigt R. and Thomas, L. Murray. "Breaking Strength of the Human Skull vs. Impact Surface Curvature," Report DOT HS-801002, National Technical Information Service, Springfield, Virginia; 1973.

Hosmer, D. and Lemeshow, S. Applied Logistic Regression, John Wiley & Sons, New York; 1989.

Khalil, T. B. and Hubbard, R.P. "Parametric Study of Head Response by Finite Element Modeling," J. Biomech., 10: 119-132, Pergamon Press; 1977.

Kleiven, Svein and von Holst, Hans. "Consequences of Brain Size Following Impact in Prediction of Subdural Hematoma Evaluated with Numerical Techniques," IRCOBI Conference – Isle of Man; 2001.

Meaney, D.F. "Biomechanics of Acute Subdural Hematoma in the Sub-Human Primate and Man," Ph.D. thesis, University of Pennsylvania; 1991.

Newman, James A. "A proposed new biomechanical head injury assessment function - the maximum power index," 44th Stapp Car Crash Conference, SAE 2000-01-SC16; 2000.

Patrick, Lawrence M., Lissner, Herbert R. and Gurdjian, E.S. "Survival by Design – Head Protection," 7th Stapp Car Crash Conference, SAE 1963-12-0036, 1963

S.A.E. "Instrumentation for Impact Test – Part 1-Electronic Instrumentation," Surface Vehicle Information Report, Society for Automotive Engineers, Warrendale, Pa, J211-1; 1995.

Stata Users Guide. (1999). Stata Press, College Station, TX.

Thibault, L.E., Galbraith, H.A., Thompson, C.J. and Gennarelli, T.A. "The Effects of High Strain Rate Uniaxial Extension on the Electrophysiology of Isolated Neural Tissue," Advances in Bioengineering, D. Viano (ed.), ASME, New York; 1982.

U.S. Code of Federal Regulations, Title 49 (Transportation), Part 571.208 (Federal Motor Vehicle Safety Standards); 2002.

Yoganandan N, Maiman DJ, Pintar FA, Ray G, Myklebust JB, Sances A Jr, Larson SJ: "Microtrauma in the lumbar spine: A cause of low back pain," Neurosurgery 23(2):162-168, 1988.

Wood, J. L. "Dynamic Response of Human Cranial Bone," J. Biomech. 4: 1-12; 1971.

Zhang, L, Yang, K.H., Dwarampudi, R., Omori, K., Li, T., Chang, K., Hardy, W.N., Khalil, T.B. and King, A.I. "Recent Advances in Brain Injury Research: A New Human Head Model Development and Validation," SAE 2001-22-0017, P-375, 45th Stapp Car Crash Conference; 2001.